Ages and cooling history of the Early Cretaceous Caleu pluton: testimony of a switch from a rifted to a compressional continental margin in central Chile

M.A. Parada, G. Féraud, F. Fuentes, L. Aguirre, D. Morata

Ages and cooling history of the Early Cretaceous Caleu pluton: testimony of a switch from a rifted to a compressional continental margin in central Chile

MIGUEL A. PARADA[1], GILBERT FÉRAUD[2], FRANCISCO FUENTES[1], LUIS AGUIRRE[1], DIEGO MORATA[1] & PAULA LARRONDO[1]

[1]*Departamento de Geología, Universidad de Chile, Casilla 13518, Santiago, Chile (e-mail: maparada@cec.uchile.cl)*

[2]*Géosciences Azur, UMR 6526, CNRS–Université de Nice–Sophie Antipolis, 06108 Nice Cedex 02, France*

Abstract: The Caleu pluton, in the Coastal Range of central Chile, represents the last magmatic event related to the Early Cretaceous rifting along the western margin of South America. The pluton was emplaced into a *c*. 10 km thick pile of mainly basalts and basaltic andesites deposited in an Early Cretaceous subsiding basin, and affected by very low-grade metamorphism. The cooling history of the pluton is documented on the basis of U–Pb, $^{40}Ar/^{39}Ar$ step-heating and fission-track dating. The U–Pb date suggests an age of emplacement in the interval 94.2–97.3 Ma. Rapid subsolidus cooling between 550–500 °C and 250 °C is documented by $^{40}Ar/^{39}Ar$ plateau ages on amphibole, biotite and plagioclase between 94.9 ± 1.8 and 93.2 ± 1.1 Ma. Slower subsolidus cooling to *c*. 100 °C is identified at the 94–90 Ma interval by the fission-track thermal model. The geochronological data show that the emplacement of the pluton is coeval with the very low-grade metamorphism of the host rocks. Therefore, this metamorphism is probably not the result simply of burial, but also of a regional thermal gradient related to the plutonism. Exhumation of the pluton started coevally with its emplacement and continued to about 90 Ma, being associated with the closure of the Early Cretaceous rifting. The Caleu plutonism represents an asthenospheric-derived event during maximum extension, and marks a turning point between extensional- and compressional-related magmatism.

Keywords: Chile, Caleu pluton, absolute age, exhumation, extension.

Widespread rifting and generation of ensialic basins from Colombia in the north to southernmost Chile are the most outstanding features characterizing the evolution of the active western margin of South America during the Cretaceous. These events have been interpreted as the outcome of trench retreat that led to partial or total crustal attenuation at the continental margin (Pankhurst *et al*. 1988), asthenospheric upwelling to fill the gap (Aguirre *et al*. 1989), bimodal volcanism, subsidence, burial metamorphism and plutonic activity (Åberg *et al*. 1984; Vergara *et al*. 1995; Aguirre *et al*. 1999). The imprints of such events are at present recorded as volcano-plutonic lineaments extending for thousands of kilometres along the Andean Range (Dalziel 1981; Åberg *et al*. 1984; Aguirre *et al*. 1989).

In Peru, this type of lineament is represented by the West Peruvian Trough, which evolved by 'encratonic' spreading involving marginal basin development (Atherton *et al*. 1983, 1985). A composite marginal basin (Huarmey–Cañete) was the site of intense volcanism, which deposited upwards of 9000 m of volcanic and volcanogenic material from the Tithonian to the Albian, with maximum subsidence in the Albian (Atherton *et al*. 1985). These rocks were later affected by low-grade metamorphism under high geothermal gradients. The lineament-constrained multiple Peruvian Coastal Batholith forms the core of the Western Cordillera, occupying, for the most part, a *c*. 50 km wide band lying within the exposed Albian rocks of the marginal basin (see Pitcher & Cobbing 1985; Atherton 1990).

In north and north–central Chile, between latitudes 25°S and 36°S, bimodal volcanic activity took place along the rifted continental margin during the Early Cretaceous (*c*. 120 Ma), generating a *c*. 1200 km long uninterrupted belt with an average width of 30 km and thickness of 3–13 km. These volcanic rocks were later affected by a very low-grade metamorphic event dated in adularia at 93.1 ± 0.6 and 94.2 ± 1.2 Ma (Aguirre *et al*. 1999). Granitoid complexes with ages around 90–96 Ma, bearing a chemical mantle signature akin to the volcanic material, are spatially related to this volcanic belt.

In Chile, the temporal relationships between the granitoids, the basinal volcanic rocks, the metamorphic phenomena, and the exhumation of these volcano-plutonic lineaments have been poorly explored. In north–central and central Chile, the inception of extensional basins during the Cretaceous and their subsequent evolution is the most outstanding orogenic event of the Mesozoic, which led to the rise of the Andean mountain chain along this margin of South America.

The aim of this study is to provide evidence from zircon U–Pb, hornblende, biotite and plagioclase $^{40}Ar/^{39}Ar$, and apatite fission-track dating about the timing of magmatism and subsolidus cooling of the Caleu pluton, a *c*. 340 km^2 composite intrusion emplaced in a Lower Cretaceous succession affected by very low-grade metamorphism. The geological setting of the pluton is favourable for establishing temporal relationships between the plutonism, the very low-grade metamorphism of the volcanic host rocks and the tectonic processes that took place during the Early Cretaceous, a key period of the Andean geodynamic evolution in central Chile.

Geological setting

The Early Cretaceous magmatism of the Coastal Range segment (32°30′– 33°30′S) of central Chile is represented by the Caleu pluton and its host volcanic–sedimentary succession (Fig. 1). The Caleu pluton is a good example of the numerous Early Cretaceous plutons of the Coastal Batholith of central Chile. These Early Cretaceous plutons form part of one of the largest Andean magmatic provinces, which extends as a continuous belt for over *c*. 750 km, from 27° to 34°S. In the studied segment of

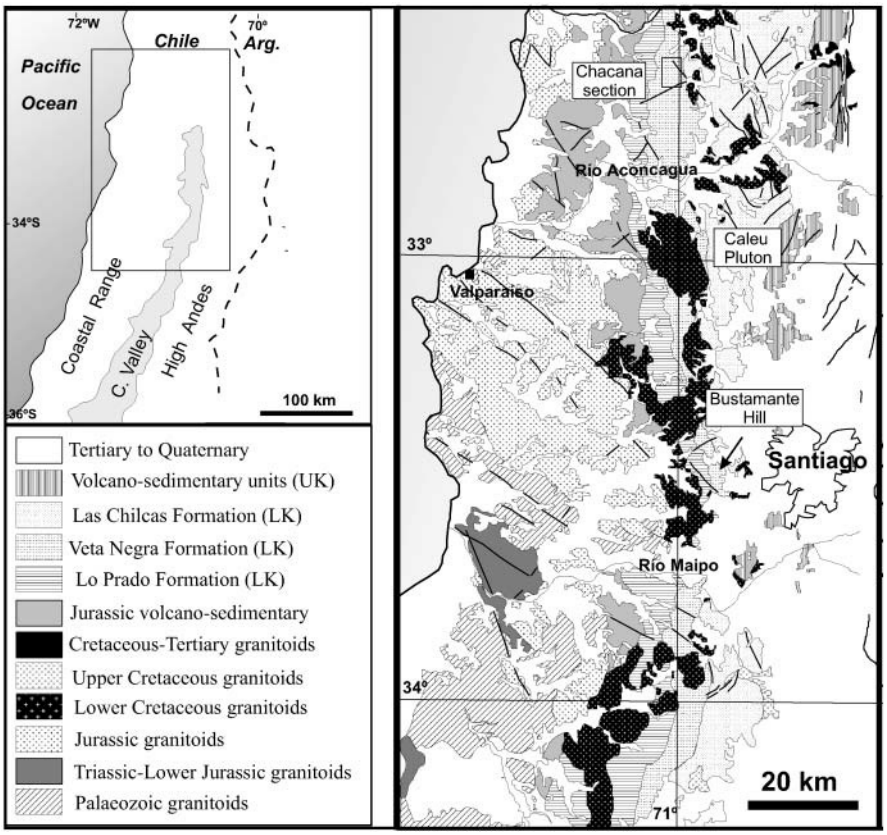

Fig. 1. Geological setting of the Caleu pluton.

the Coastal Range, Early Cretaceous granitoids and volcanic rocks crop out over an area of more than 6000 km^2. The Early Cretaceous plutonism corresponds to the eastern belt of the Coastal Batholith segment, which is made up of three north–south belts with age decreasing eastward from late Palaeozoic to Jurassic to Early Cretaceous.

The Caleu pluton is emplaced into a thick Early Cretaceous volcanic–sedimentary arc succession deposited in a subsiding basin (Fig. 2; Vergara *et al*. 1995). This succession includes the Ocoite Group (Aguirre *et al*. 1989) and the Las Chilcas Formation (Thomas 1958). At the latitude of Santiago (33°S) the Ocoite Group is represented by a *c*. 15 km thick succession, tilted to a dip of 30–40°E. Its lower third (the Valanginian to Hauterivian Lo Prado Formation) consists of marine and continental volcanic sedimentary rocks, limestones, and a bimodal succession of dacitic ignimbrites and interbedded basalts. The

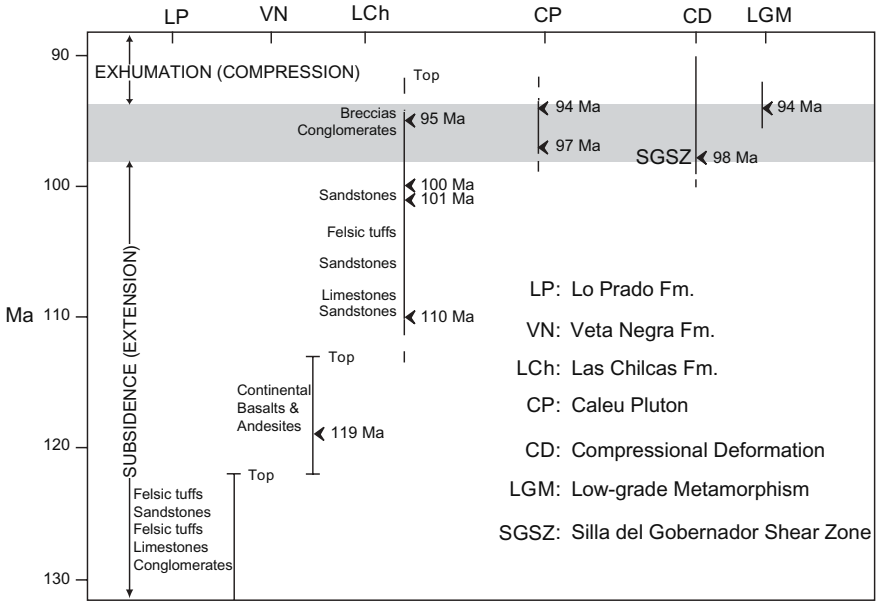

Fig. 2. Summary of the stratigraphic and tectonic events during the Early Cretaceous evolution of the Coastal Range of central Chile. Bracketed ages are based on stratigraphic controls. The geochronological data given here were obtained from Aguirre *et al*. (1999), Wall *et al*. (1999), Arancibia (pers. commun.) and this study.

central part of the group is the *c*. 5–10 km thick (see Vergara *et al*. 1995) Hauterivian to Barremian Veta Negra Formation, which is made up of subaerial porphyritic basalts and basaltic andesites with high-K to shoshonitic affinity (Levi & Aguirre 1981; Åberg *et al*. 1984; Levi *et al*. 1988; Vergara *et al*. 1995). The uppermost part consists of continental flow-breccias of basaltic andesite to andesite composition and sedimentary clastic intercalations. The Veta Negra Formation has been affected by very low- to low-grade burial metamorphism in an extensional geodynamic setting (Aguirre *et al*. 1999).

$^{40}Ar/^{39}Ar$ ages of about 119 ± 2.4 Ma have been obtained on primary plagioclase in basaltic flows of the Veta Negra Formation at the Bustamante Hill section, 35 km south of the Caleu pluton (Aguirre *et al*. 1999). In the vicinity of the Caleu pluton, the Las Chilcas Formation consists of a succession of limestones, red sandstones, andesites, rhyolitic tuff intercalations and thick strata of coarse volcano-sedimentary breccias and conglomerates, which conformably overlies the Veta Negra Formation. Unlike that formation, the Las Chilcas Formation does not exhibit a widespread metamorphic mineralogy attributable to very low-grade metamorphism, although the coarse conglomerates contain abundant very low-grade metavolcanic rock clasts. A mid-Albian (*c*. 105 Ma) age has been recorded from marine planktonic microfossils found in limestones at the lower levels of the Las Chilcas Formation (Martínez-Pardo *et al*. 1994). Recently, Wall *et al*. (1999) have obtained zircon U–Pb ages in felsic volcanic rocks of the lower section of the Las Chilcas Formation in the 109.6 ± 0.2 to 106.5 ± 0.4 Ma range. These ages are older than the corresponding whole-rock K–Ar ages of 101 ± 3 and 100 ± 3 Ma (near the Bustamante Hill section) and plagioclase K–Ar age of 95 ± 3 Ma (near the Caleu pluton) obtained in lavas of the upper stratigraphic levels of the Las Chilcas Formation (Wall *et al*. 1999). A biotite K–Ar age of 91 ± 4 Ma has been obtained for the Caleu pluton (Gana *et al*. 1996) indicating that it represents a magmatic event contemporaneous with the deposition of the upper section of the Las Chilcas Formation.

Geology of the Caleu pluton

The Caleu pluton, located in the Coastal Range of central Chile *c*. 40 km NW of Santiago, has a subrectangular shape (Fig. 3), good exposures and >1400 m of vertical relief. The western margin of the pluton is the contact with the Early Cretaceous La Campana gabbro stock and with felsic volcanic rocks of the Valanginian–Hauterivian Lo Prado Formation. The southern and northern margins of the pluton intrude the Veta Negra Formation, whereas its eastern margin is well defined only along a nearly north–south fault contact with rocks of the lower section of the Las Chilcas Formation. Pressures of emplacement of the pluton of *c*. 2.0 kbar were calculated using the Al-in-hornblende geobarometer in more than 10 representative samples containing quartz, plagioclase, K-feldspar, hornblende, biotite, sphene and magnetite (Parada *et al*. 2002).

The Caleu pluton consists of three north–south elongated zones (Fig. 3), with contacts that dip subvertcally. The three zones, which define an across-pluton compositional variation characterized by a westward increase in SiO_2 content, are the Gabbro–Diorite Zone, Tonalite Zone and Granodiorite Zone.

The Gabbro–Diorite Zone has a north–south elongated shape, which occupies 140 km^2 at the eastern part of the pluton. It includes coarse-grained gabbros and diorites having a colour index between 18 and 30, because of the presence of clinopyroxene, hornblende and biotite.

Amphibole–biotite-bearing tonalites and quartz diorites are most abundant in the Tonalite Zone, and cover the central part of the pluton as a north–south belt of *c*. 70 km^2. The contact between Tonalite Zone and Gabbro–Diorite Zone appears to be gradational, as indicated by a progressive decrease in the colour index (15–20) and in the grain size to medium-grained rocks. However, in some places small batches of quartz diorite intrude rocks of the Gabbro–Diorite Zone. A distinct feature of this zone is the presence of rounded dioritic enclaves of variable size from 5 to 40 cm.

The Granodiorite Zone covers 30 km^2 at the western part of the body and it extends towards the east as a subhorizontal sill of *c*. 100 m thick, hosted within the Tonalite Zone. Intrusions of small Granodiorite Zone bodies into the Gabbro–Diorite Zone were also observed in the eastern part of the pluton. Unlike the gabbros and diorites, the granodiorites are leucocratic with a colour index between 5 and 10 resulting from the presence of minor amphibole and biotite.

Palaeomagnetic studies in the Caleu pluton (Parada *et al*. 2002) indicate normal polarity of the remanent magnetization, which is consistent with the long normal polarity Cretaceous superchron. The pluton has a declination of 9.6° and an inclination of −56.6°, which are slightly different from the expected values of 350° and −54.8°, respectively, for Cretaceous rocks. These differences have been explained by a 10–15° tilt of the pluton toward the east or by a 10–20° clockwise rotation. The remagnetized Lo Prado and Veta Negra strata (dipping 30° and *c*. 80° SW, respectively) at the southwestern margin of the pluton have the same *in situ* palaeomagnetic direction as those recorded in the adjacent plutonic rocks, suggesting that the pluton intruded the host volcanic formations after their tilting.

Ocoite Group: lithological and metamorphic features

In Bustamante Hill (*c*. 33°30′S; Fig. 1) the lowest stratigraphic level of the Ocoite Group corresponds to strata of the Lo Prado Formation, *c*. 2000 m thick, which consist of marine and continental clastic rocks, limestones, and a succession of dacitic ignimbrites and basaltic andesites (Fig. 2; Levi 1969). These rocks have been affected by low-grade non-deformative metamorphism characterized by greenschist-facies mineral assemblages (Levi 1969).

The Veta Negra Formation overlies the Lo Prado Formation between the Bustamanate Hill and Chacana areas (*c*. 32°40′S; Fig. 1). It is mainly composed of a pile of *c*. 5–10 km thick basaltic andesites and andesites (Levi 1969; Levi *et al*. 1982; Vergara *et al*. 1995), with a distinct porphyritic texture characterized by abundant and large (up to 2 cm) Ca-plagioclase phenocrysts, subordinate augite, titanomagnetite and small amounts of altered olivine crystals.

The rocks of the Veta Negra Formation have been affected by very low-grade, non-deformative metamorphism. The proportion of secondary minerals (in veinlets, amygdules, and primary mineral and glass replacement) increases downward in the pile, and the mineral assemblages characterize a gradual change of metamorphic facies from a pumpellyite-bearing zeolite facies at the top to a prehnite–pumpellyite facies in the middle and bottom (Levi *et al*. 1989). Regional metamorphic facies boundaries are parallel or subparallel to bedding and not to the exposed contacts with contemporaneous or younger granitoids in the area. Based on the physical conditions of the metamorphism, Aguirre *et al*. (1989) calculated a thermal gradient of around 20–30 °C km^{-1}. However, a gradient of about 40–45 °C km^{-1} is deduced from the *P–T* conditions of the very low-grade

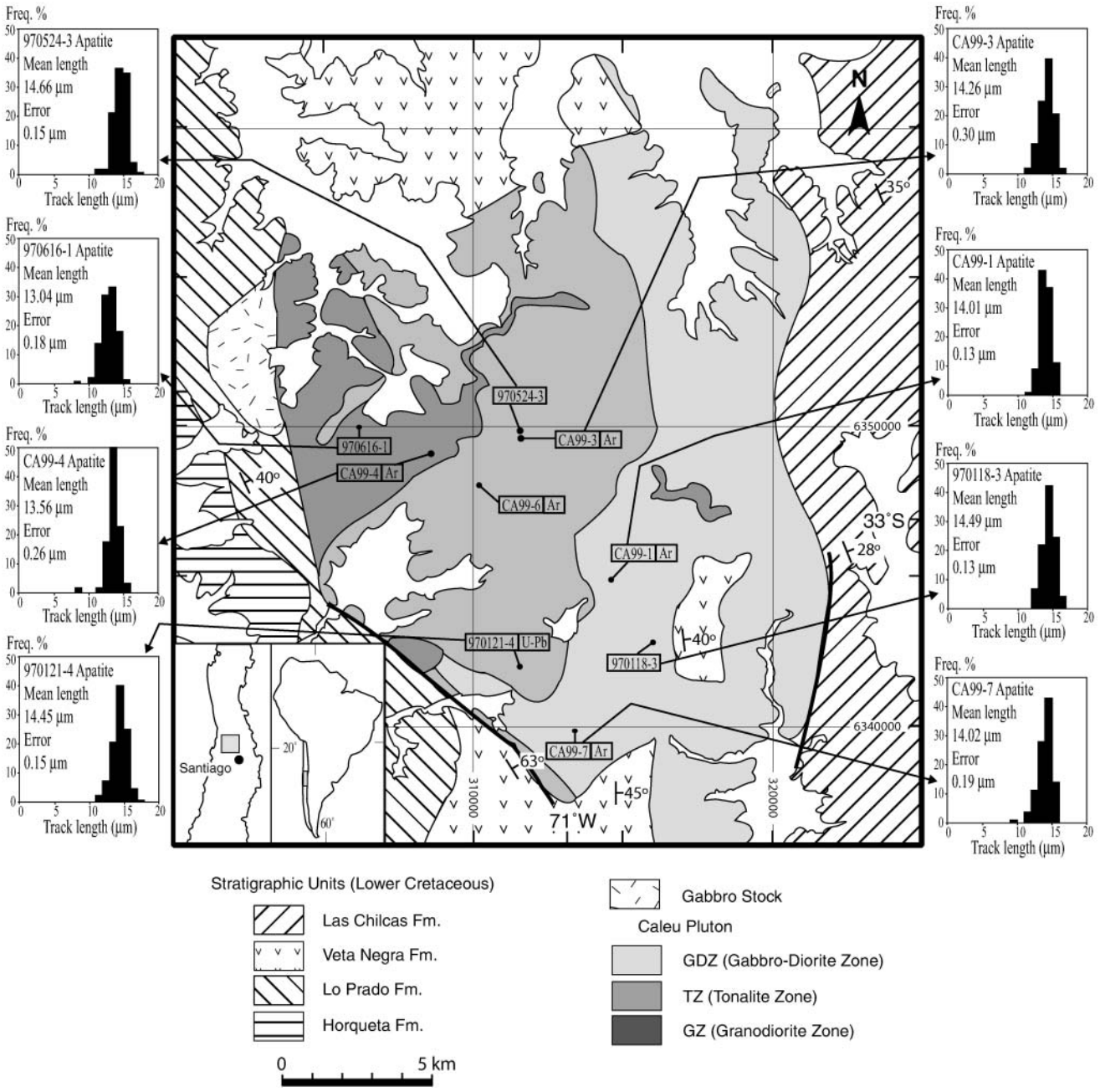

Fig. 3. Geological map of the Caleu pluton and location of dated samples. Histograms show measured track length for apatite of samples from the Caleu pluton.

metamorphism obtained from low-variance assemblages contained in amygdules of Veta Negra lavas (Aguirre *et al*. 1999).

Analytical procedures for $^{40}Ar/^{39}Ar$ and fission-track dating

$^{40}Ar/^{39}Ar$ dating

Samples from the Caleu pluton were analysed by the $^{40}Ar/^{39}Ar$ step heating procedure on single grains of amphibole and biotite, a cluster of four grains of amphibole, and bulk samples of plagioclase. The samples were altered to different degrees, and we chose to analyse single grains despite the resulting increased errors. Grain sizes for single-grain and multi-grain analyses are of the order of 180–500 µm long. The grain sizes for the plagioclase bulk samples are 250–500 µm long and the analysed weight was 35–42 mg. Single grains of amphibole were separated using a magnetic separator and heavy liquids; biotite crystals were hand picked from crushed whole rocks; and plagioclases were separated using a magnetic separator, then carefully selected under a binocular microscope, so as to select only transparent grains. The samples were irradiated in the nuclear reactor at McMaster University (Hamilton, Canada), in position 5c. The total neutron flux density during irradiation was 8.8×10^{18} n cm^{-2}, with a maximum flux gradient estimated at ±0.2%. We used the Fish Canyon sanidine (FCs) as a flux monitor with an age of 28.02 Ma (Renne *et al*. 1998). The plagioclase bulk sample analyses were performed with a mass spectrometer composed of a 120° M.A.S.S.E. tube, a Baür–Signer GS 98 source and a Balzers electron multiplier. The gas extraction of single grains and small

clusters of grains was carried out by heating with a Synrad 48-5 CO_2 laser. The mass spectrometer used was a VG 3600 working with a Daly detector system. Typical blank values of the extraction and purification laser system are in the range $(30–90) \times 10^{-14}$, $(0.3–8) \times 10^{-14}$, $(10–20) \times 10^{-14}$, and $(0.3–7) \times 10^{-14}$ cm^3 STP (standard temperature and pressure conditions) for the masses ^{40}Ar, ^{39}Ar, ^{37}Ar and ^{36}Ar, respectively, measured every third step. The criteria for defining plateau ages were the following: (1) it should contain at least 70% of released ^{39}Ar; (2) there should be at least three successive steps in the plateau; (3) the integrated age of the plateau should agree with each apparent age step of the plateau within a 2σ error confidence interval. Uncertainties on the apparent ages of each step (see Table 3 and age spectra) are quoted at the 1σ level and do not include the errors of the age of the monitor. All other quoted uncertainties are given at the 2σ level. The error of the $^{40}Ar^*/^{39}Ar_K$ ratio of the monitor is included in the plateau age error calculation. We present here only data giving plateau ages.

Fission-track dating

Apatite separates from seven samples were mounted in epoxy and polished to expose internal grain surfaces. Spontaneous fission tracks were revealed by etching in 5M HNO_3 for 20 s at 24 °C. Fission-track ages were determined using the external detector method (Hurford & Green 1982). A thin sheet of low-uranium muscovite was placed in contact with the polished surface of each grain mount to serve as a detector of neutron-induced fission. Samples were irradiated at the Dalhousie University Slowpoke reactor in the presence of a glass neutron dosimeter of known characteristics.

Track densities for both spontaneous and induced fission-track populations were counted at 1000× magnification. Fission-track ages were calculated using a weighted mean zeta calibration factor (Fleisher *et al*. 1975; Hurford & Green 1982), determined using the Fish Canyon Tuff apatite (obtained from C. W. Naeser) and Durango apatite (obtained commercially) age calibration standards.

Geochronological results of the Caleu pluton

Nine samples of plutonic rocks were selected for dating (Fig. 2). Eight of them were collected to provide cooling ages, and one sample was selected to date the emplacement of the pluton by the U–Pb method. Five samples were dated by the step heating $^{40}Ar/^{39}Ar$ method on minerals, and seven by apatite fission-track techniques. Sample locations and descriptions are given in Figure 3 and Table 1, respectively.

U–Pb results

Single-grain zircon analyses were carried out at the MIT laboratory for the Tonalite Zone sample 970121-4, following the procedures given by Schmitz & Bowring (2001). This sample was collected from the southernmost outcrops of this zone and at the lowest elevation (850 m; Table 1). Six grains were analysed (Table 2) and the results are shown in the concordia diagram (Fig. 4). Four of the five clustered data (z1, 3, 4, 5, 7) lie on the concordia (z3, 4, 5, 7), but they are not identical in age, spreading over about 3 Ma along the curve. Therefore we are unable to give an anambiguous U–Pb age for this sample. Nevertheless, it is likely that the age is bracketed in the interval 94.2–97.3 Ma.

$^{40}Ar/^{39}Ar$ results

Amphibole. One amphibole single grain from gabbro (CA99-7) displayed a plateau age of 95.0 ± 2.8 Ma followed by a very high apparent age (last step) that may be caused by excess argon (Fig. 5), possibly trapped in an inclusion. The variable $^{37}Ar_{Ca}/^{39}Ar_K$ ratios, the ranging from of 4 to 30, demonstrate that the analysed grain is not pure. This ratio, calculated from CaO/K_2O ratios measured by electron microprobe analysis (EMPA; $CaO/K_2O = 2.179 \times {}^{37}Ar_{Ca}/{}^{39}Ar_K$), varies between 9.1 and 12.6.

Two small amphibole grains from tonalite sample CA99-3 gave plateau ages of 92.1 ± 4.6 and 96.0 ± 3.9 Ma, affected by large error bars. Both age spectra are characterized by a rather constant $^{37}Ar_{Ca}/^{39}Ar_K$ ratio (*c*. 13) with a value close to the EPMA ratio (8–10). A single amphibole grain from sample CA99-6, of the same Tonalite Zone, displays a perturbed age spectrum giving a plateau age of 93.2 ± 1.1 Ma. The $^{37}Ar_{Ca}/^{39}Ar_K$ ratio spectrum is variable and contains only two successive steps with values similar to the EPMA ratio. The large error bars are explained by the small size of the amphibole grain. A group

Table 1. *Summary of the petrographic features and sampling elevation of the dated samples*

Sample	Rock type	Zone	Dating method	Mineral components and textures	Observation/alteration	Elevation (m)
CA99-1	Norite	GDZ	Ar/Ar (bt), FT	Mesocumulate zoned pl; interstititial opx, bt, mt, ap, ± hb	Unaltered	1080
CA99-7	Diorite	GDZ	Ar/Ar (bt, hb), FT	Orthocumulate zoned pl, interstitial bt, hb, qz, mt, opx, ap	Some bt crystals are chloritized. Some hb crystals are poikilitic and have cpx core. Pl crystals are slightly sericitized	1070
970118-3	Qz-monzodiorite	GDZ	FT	Mesocumulate zoned pl; interstititial qz, K-feld, bt, hb, mt, ap	Unaltered	1410
970121-4	Qz-diorite	TZ	U–Pb, FT	Orthocumulate zoned pl, interstitial K-feld,bt, hb, qz, mt, ap, mt, zr	Unaltered. Some hb crystals are replacing cpx	855
CA99-3	Qz-monzodiorite	TZ	Ar/Ar (bt,hb,pl)	Equigranular. Zoned pl, qz, K-feld, bt, hb, mt, ap, small amount of opx	Hb crystals are commonly poikilitic and zoned	2075
970524-3	Tonalite	TZ	FT	Equigranular. Zoned pl, qz, bt, hb, small amount of K-feld, ap, sph, zr, mt	Unaltered. Some hb crystals are replacing cpx	1975
CA99-6	Tonalite	TZ	Ar/Ar (hb)	Equigranular. Zoned pl, qz, hb, bt, minor amount of K-feld, mt, ap, sph, zr	Some bt crystals are chloritized. Fine-grained hb crystals	1640
CA99-4	Granodiorite	GZ	Ar/Ar (hb), FT	Porphyric. Phenocrysts: Zoned pl, hb, bt. Felsitic matrix, ap, mt, mt	Unaltered hb. Bt partially chloritized	1420
970616-1	Granite	GZ	FT	Porphyric. Phenocrysts: Zoned pl, hb, bt. Felsitic matrix, ap, mt, mt	Unaltered. Some hb crystals are replacing cpx	1110

GDZ, Gabbro-Diorite Zone; TZ, Tonalite Zone; GZ, Granodiorite Zone; FT, fission track; pl, plagioclase; hb, hornblende; bt, biotite; cpx, clinopyroxene; opx, orthopyroxene; qz, quartz; K-feld, K-feldspar; mt, magnetite; ap, apatite; zr, zircon.

Table 2. *U-Pb geochronological data for zircons from the Caleu pluton (sample 970121-4)*

Fraction	Weight (mg)	Concentration		$^{206}Pb^*/^{204}Pb$	$^{208}Pb/^{206}Pb$	$^{206}Pb^\dagger/^{238}U$	% Error	$^{207}Pb^\dagger/^{235}U$	% Error	$^{207}Pb^\dagger/^{206}Pb$	% Error	Isotopic ages (Ma)			Corr. coeff.	$Pb^\ddagger$ (pg)	$Pb^*/Pb^\ddagger$
		U (ppm)	Pb (ppm)									$^{206}Pb/^{238}U$	$^{207}Pb/^{235}U$	$^{207}Pb/^{206}Pb$			
z4	0.1227	148.6	2.5	3463	0.250	0.01513	0.43	0.10022	0.47	0.04805	0.19	96.8	97	101.5	0.92	5.1	60.0
z5	0.154	80.1	1.3	3465	0.257	0.01496	0.11	0.09884	0.17	0.0479	0.13	95.8	95.7	94.5	0.66	3.4	60.1
z3	0.1733	101.2	1.7	3127	0.254	0.01481	0.53	0.09787	0.57	0.04794	0.22	94.8	94.8	96.1	0.93	5.4	54.3
z7	0.0237	225.7	3.7	6433	0.229	0.01475	0.21	0.09742	0.24	0.04792	0.11	94.4	94.4	95.2	0.89	0.8	109.6
z1	0.1613	101.9	1.7	1910	0.222	0.01468	0.36	0.09741	0.52	0.04811	0.36	94.0	94.4	104.9	0.72	8.2	32.3
z6	0.0407	137.1	2.0	1196	0.269	0.01249	0.76	0.08256	0.97	0.04793	0.57	80.0	80.6	95.8	0.81	3.8	20.8

Blank isotopic composition: $^{206}Pb/^{204}Pb = 19.10 \pm 0.1$, $^{207}Pb/^{204}Pb = 15.72 \pm 0.1$, $^{208}Pb/^{204}Pb = 38.65 \pm 0.1$. All errors are reported as 2σ. Sample weights are estimated using a video monitor with gridded screen and are known to within 40%. Common Pb corrections were calculated using the model of Stacey & Kramers (1975) and the interpreted age of the sample. Total procedural Pb and U blanks were 0.65–2.0 pg and <1.0 pg, respectively.
*Measured ratio corrected for spike and fractionation only. Mass fractionation correction of 0.15% a.m.u. $^{-1} \pm 0.04\%$ a.m.u. $^{-1}$ was applied to all analyses.
†Corrected for fractionation, spike, blank and initial common Pb.
‡Total common Pb in analyses.

of four amphibole crystals from granodiorite sample CA99-4 yields a well-defined plateau age at 93.7 ± 0.6 Ma. The relatively constant $^{37}Ar_{Ca}/^{39}Ar_K$ ratios with values around five closely approach the EPMA ratios of 6–10.

Biotite. Laser-probe analyses were carried out on five single grains of biotite from three samples. The $^{40}Ar/^{39}Ar$ age spectra displayed by the biotites from a sample of gabbro CA99-1 give two well-defined plateau ages of 94.3 ± 1.4 and 93.4 ± 0.8 Ma (Fig. 5). Two biotites from gabbro located near the pluton margin (sample CA99-7) gave more disturbed age spectra, which, nevertheless, define plateau ages of 96.0 ± 0.6 and 96.0 ± 0.8 Ma. These slight disturbances may be the result of a weak chloritization of the mineral that is observed in thin sections. A small grain of biotite from tonalite (sample CA99-3) also yielded a disturbed age spectrum, but still defined a plateau age of 94.9 ± 1.8 Ma.

Plagioclase. A plagioclase bulk sample from tonalite CA99-3 displays a plateau age of 94.0 ± 0.3 Ma containing over 80% of the ^{39}Ar released (Fig. 5). This age is concordant with the $^{36}Ar/^{40}Ar$ v. $^{40}Ar/^{39}Ar$ correlation diagram age of 93.7 ± 0.6 Ma (not shown; initial $^{40}Ar/^{36}Ar$ ratio of 296.8 of atmospheric composition, MSWD = 2.5) calculated on the plateau fraction. The $^{37}Ar_{Ca}/^{39}Ar_K$ ratio ranges from 0.2 to 2.0.

Detailed $^{40}Ar/^{39}Ar$ analytical results for biotites, amphiboles and plagioclases are given in Table 3.

Fission-track results

Apatite mineral separates from two gabbros (970118-3, CA99-1), three tonalites (970121-4, 970524-3, CA99-7) and two granodiorites (970616-1, CA99-4) from the samples dated by $^{40}Ar/^{39}Ar$ were dated by the fission-track method. Apatite in three samples contained substantial dislocations and pitting, and was variously zoned. The apatite fission-track age data given in Table 4 are therefore considered to be highly reproducible. The pooled fission-track ages (error at the 2σ level) of the samples are: 92.7 ± 6.2 Ma and 93.1 ± 2.6 Ma for the Gabbro–Diorite Zone samples; 90.4 ± 7.6 Ma, 95.7 ± 6.2 Ma and 96.5 ± 5.4 Ma for the Tonalite Zone samples; and 82.0 ± 5.6 Ma and 91.9 ± 5.1 Ma for the Granodiorite Zone samples. Six of the analysed samples contain very long (unannealed) confined tracks, and a long mean confined track length, indicating that these samples cooled relatively rapidly. The oldest age (CA99-7) is based on only seven relatively dislocation-free grains. Most of the ages reported here are very similar to the previous apatite fission-track age of 91 ± 3.2 Ma reported by Gana & Zentilli (2000) for the same pluton. In addition, the ages of the Caleu pluton are close to apatite fission-track ages obtained on Jurassic and Palaeozoic granitoids (98 ± 10 to 106 ± 8 Ma; Gana & Zentilli 2000) that crop out *c*. 70 km west of the Caleu pluton, along the coastline south of Valparaiso.

Interpretation and tectonic significance of the geochronological data

Magmatism and regional thermal history

A magmatic quiescence is recognized between the Veta Negra volcanism and the Caleu plutonism. In fact, plagioclases from basaltic flows of the Veta Negra Formation at the Bustamante Hill and Chacana sections have been dated around 119 ± 1.2 Ma by the $^{40}Ar/^{39}Ar$ method (Aguirre *et al*. 1999; Fuentes *et al*.

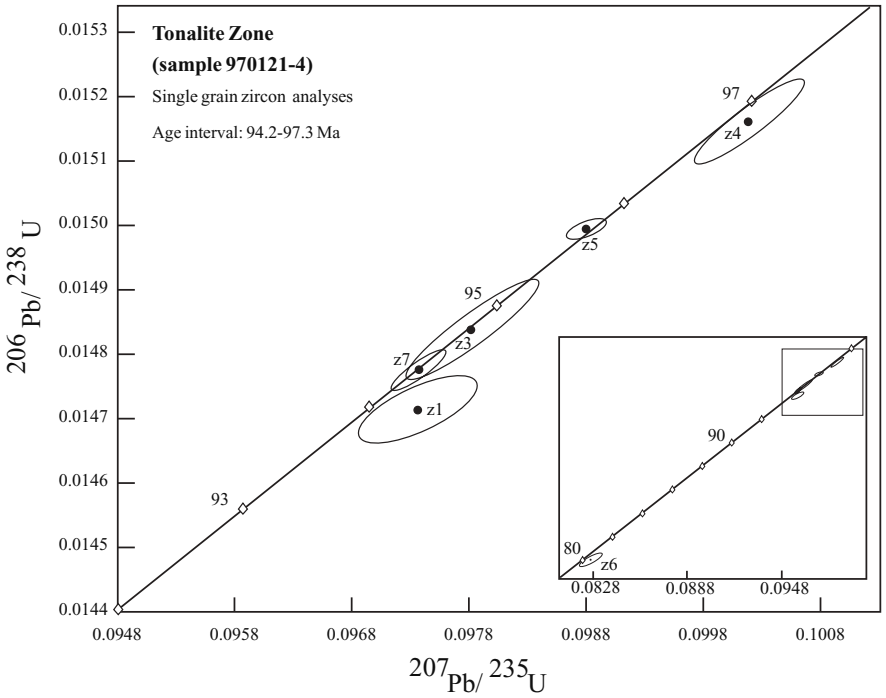

Fig. 4. U–Pb concordia diagram for single-grain zircon analyses of the Caleu pluton. Labels correspond to analysed zircon fraction in Table 2.

2001), which are about 24 Ma older than the Caleu pluton (Fig. 2). The only magmatic activity occurring between these two events is the small volume of andesites, rhyolite and volcaniclastic intercalations in the lower and upper sedimentary section (*c*. 110–106 and 101–95 Ma, respectively) of the Las Chilcas Formation.

From geochronological data (*c*. 94 Ma) obtained on minerals in equilibrium with peak burial conditions of metamorphism, Aguirre *et al*. (1999) proposed that the very low-grade metamorphism of the Veta Negra flows was the result of burial conditions only, and was not related to the numerous and large igneous bodies (including the Caleu pluton) intruding the Veta Negra Formation. This hypothesis was supported by the fact that the metamorphic mineral assemblages are a direct function of the stratigraphic depth (Levi 1969; Aguirre *et al*. 1989; Levi *et al*. 1989), and are not conformable with exposed boundaries of the pluton. However, without any precise knowledge of the emplacement age of the pluton and the age of the metamorphism of the host rocks, it was hard to establish any reliable time relationship between them. The geochronological data obtained for the Caleu pluton clearly show that its emplacement and cooling (dated between 93.2 ± 1.1 and 94.9 ± 1.8 Ma) is coeval with the low-grade metamorphism (Fig. 2) dated between 93.5 ± 0.6 and 94.2 ± 1.2 Ma by $^{40}Ar/^{39}Ar$ on adularia in the Bustamante Hill section of the Veta Negra Formation (Aguirre *et al*. 1999). Therefore, the low-grade metamorphism dated may not be the result of burial alone, but may also involve a rise in the regional thermal gradient related to at least one magmatic event. The Caleu pluton was thus emplaced at the end of the Veta Negra basin subsidence, which coincided with the peak of very low-grade burial metamorphism. It is interesting to note that the temporal and spatial relationships between plutonism and low-pressure–high-temperature metamorphism has been described elsewhere as a consequence of an underlying thermal event or as a direct product of the advection of heat caused by plutonism (see Lux *et al*. 1986; Barton & Hanson 1989). The results of our study indicate that these relationships and their thermal implications can be validly applied to the development of low- to very low-grade metamorphism.

Subsolidus cooling of the pluton

Good agreement is observed for most of the $^{40}Ar/^{39}Ar$ plateau ages obtained on biotite, amphibole and plagioclase from samples CA99-1, -3, -4, -6 (biotites CA99-7 excepted) mainly ranging from 93.2 ± 1.1 to 94.9 ± 1.8 Ma, if we exclude plateau ages affected by large error bars (concordant, nevertheless, with this age range). These ages are also coincident with the U–Pb zircon age estimated in the interval 94.2–97.3 Ma.

The significantly different plateau ages of 96.0 ± 0.6 and 96.0 ± 0.8 Ma obtained on biotites from sample CA99-7, the only sample located near the pluton margin, can be explained by an earlier cooling of this marginal zone of the pluton, too old ages owing to undetectable excess argon (the $^{36}Ar/^{40}Ar$ v. $^{40}Ar/^{39}Ar$ inverse isochron plots display initial atmospheric ratios), or chloritization of the biotite. Because of the concordance of precise ages obtained on amphibole (93.7 ± 0.6 Ma) and plagioclase (94.0 ± 0.3 Ma) from samples CA99-4 and CA99-3 located in the core region of the pluton, which have a estimated closure temperature of *c*. 500–550 °C (McDougall & Harrison 1999) and 250 °C (Berger & York 1981), respectively, it is unlikely that the age difference obtained on biotite of about 2 Ma, measured on core and margin of the pluton, is real. Chloritization of the CA99-7 biotite is observed in thin section, but its effect seems low, as shown by the age spectra. Nevertheless, one of the biotites gives a weighted mean age of 94.9 ± 1.1 Ma on the five high-temperature steps (corresponding to 41% of the total ^{39}Ar released), which may give a more valid age for chloritization (Ruffet *et al*. 1991).

The high concordance of U–Pb zircon age and plateau ages obtained from amphibole CA99-4 and plagioclase CA99-3 strongly argues for fast cooling of the pluton immediately after

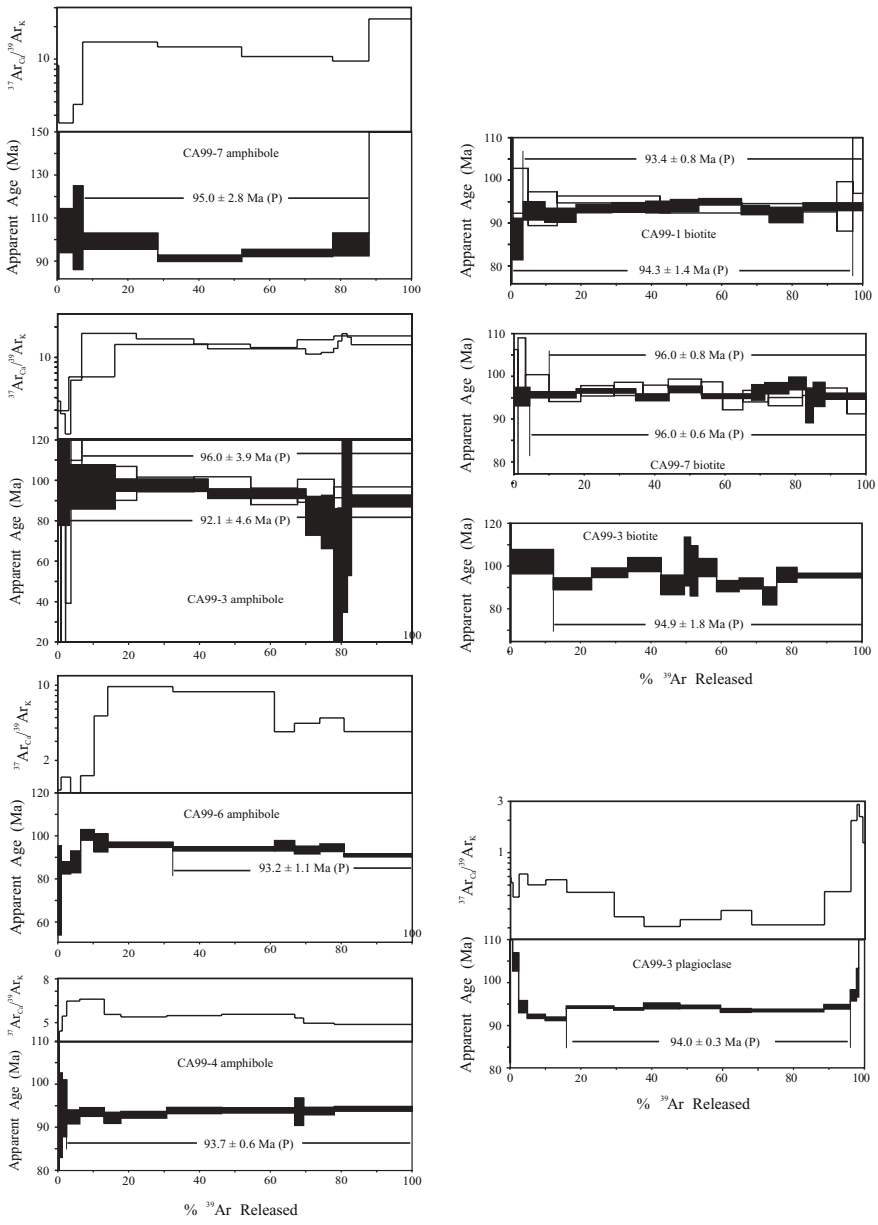

Fig. 5. Apparent age and $^{37}Ar_{Ca}/^{39}Ar_K$ ratio spectra for biotite, amphibole and plagioclase of samples from the Caleu pluton. Apparent ages and plateau ages are given at the 1σ and 2σ levels, respectively.

its crystallization, to host rock temperature at the site of emplacement (Fig. 6). This last temperature may be deduced from the thermal gradient obtained from the *c*. 93 Ma metamorphism of the Veta Negra Formation at Bustamante Hill, located about 35 km further south (Fig. 1; Aguirre *et al*. 1999). The use of this information seems justified by the homogeneity of the mineral parageneses (primary and secondary) of the Veta Negra Formation over the whole region, from Bustamante Hill to the Chacana area, 25 km north of the Caleu pluton (Fig. 1; Fuentes *et al*. 2001). Based on (1) the assumed depth of emplacement of the pluton at about 7 km (Parada *et al*. 2002), and (2) a thermal gradient of *c*. 40–45 °C km^{-1}, a temperature of the host rocks of *c*. 280–315 °C at the depth of the pluton emplacement is deduced. The rapid cooling of the pluton at *c*. 94 Ma ended only when pluton and host rocks cooled together below 250 °C (blocking temperature of Ar retention in plagioclase; see Fig. 6). Whereas U–Pb and $^{40}Ar/^{39}Ar$ data apparently indicate a rapid cooling rate of the Caleu pluton, the fission-track ages seem to correspond to a slower cooling event(s) as shown by the plots of the fission-track age data in the cooling diagram (Fig. 6).

Exhumation evidence for the Caleu pluton

An exhumation event, defined as the vertical displacement of rocks with respect to the surface (England & Molnar 1990; Stüwe & Barr 1998), may have started coevally with the emplacement of the pluton. Although the individual errors on apatite fission-track ages are too large to constrain the cooling path, a thermal model applied to three apatite sample datasets (samples CA99-1, CA99-4 and CA99-7) using a FORTRAN algorithm developed by Willett (1992, 1997) and modified by Issler (1996) allows more useful information to be obtained. Distribution of fission-track single-grain ages in the samples pass the χ^2 test. It is assumed therefore that they are composed of only one population of fission-track ages and that the age and

Table 3. *Detailed $^{40}Ar/^{39}Ar$ analytical results obtained on biotites, amphiboles and plagioclases*

Step number or T (°C)	Atmospheric contamination (%)	^{39}Ar (%)	$^{40}Ar/^{36}Ar$	$^{40}Ar/^{39}Ar$	$^{37}Ar_{Ca}/^{39}Ar_K$	$^{40}Ar^*/^{39}Ar_K$	Age (Ma)
CA99-1 biotite single grain							
1	89.24	0.29	331.16 ± 26.08	47.64 ± 0.65	0	5.129 ± 3.431	156.45 ± 100.25
2	47.30	4.63	624.51 ± 36.79	6.00 ± 0.03	0.0076 ± 0.0009	3.146 ± 0.174	97.56 ± 5.25
3	13.36	8.25	2207.46 ± 599.73	3.49 ± 0.01	0.0096 ± 0.0005	3.007 ± 0.130	93.37 ± 3.95
4	5.82	29.17	5069.48 ± 633.02	3.29 ± 0.01	0.0033 ± 0.0001	3.079 ± 0.026	95.53 ± 0.81
5	8.54	23.35	3451.69 ± 446.11	3.32 ± 0.01	0.0070 ± 0.0002	3.013 ± 0.038	93.53 ± 1.18
6	5.61	26.94	5253.30 ± 864.70	3.22 ± 0.01	0.0065 ± 0.0002	3.015 ± 0.032	93.59 ± 0.98
7	10.05	4.54	2932.83 ± 1601.5	3.39 ± 0.02	0.0115 ± 0.0008	3.025 ± 0.191	93.90 ± 5.78
Fuse	2.17	2.82	13559.57 ± 9856.6	3.51 ± 0.02	0.0035 ± 0.0014	3.413 ± 0.287	105.60 ± 8.65
							Integrated age = 94.9 ± 0.8 Ma
CA99-1 biotite single grain							
1	52.33	0.62	564.4 ± 59.1	8.31 ± 0.07	0.0181 ± 0.0029	3.958 ± 0.476	124.66 ± 14.51
2	24.83	2.81	1189.7 ± 198.3	3.62 ± 0.02	0.0057 ± 0.0009	2.710 ± 0.156	86.28 ± 4.87
3	7.92	6.24	3726.5 ± 973.3	3.18 ± 0.01	0.0039 ± 0.0004	2.923 ± 0.069	92.87 ± 2.15
4	5.13	8.84	5746.1 ± 1846.7	3.06 ± 0.01	0.0039 ± 0.0003	2.889 ± 0.053	91.83 ± 1.65
5	2.43	10.15	12119.0 ± 4910.4	3.02 ± 0.01	0.0033 ± 0.0002	2.939 ± 0.032	93.40 ± 0.99
6	1.97	9.68	14954.7 ± 8649.2	3.02 ± 0.01	0.0039 ± 0.0002	2.948 ± 0.036	93.66 ± 1.13
7	3.90	7.01	7561.4 ± 2607.3	3.08 ± 0.01	0.0046 ± 0.0003	2.951 ± 0.044	93.76 ± 1.36
8	1.84	8.05	16048.6 ± 2494.2	3.03 ± 0.01	0.0017 ± 0.0003	2.962 ± 0.046	94.08 ± 1.42
9	1.78	12.13	16553.4 ± 6744.6	3.06 ± 0.01	0.0023 ± 0.0002	2.990 ± 0.024	94.97 ± 0.76
10	3.15	7.94	9358.9 ± 3162.7	3.03 ± 0.01	0.0014 ± 0.0002	2.928 ± 0.035	93.04 ± 1.09
11	3.80	9.54	7763.6 ± 3725.6	3.02 ± 0.01	0.0017 ± 0.0003	2.892 ± 0.057	91.91 ± 1.80
Fuse	1.10	17.00	26955.5 ± 2838	3.00 ± 0.01	0.0002 ± 0.0001	2.955 ± 0.029	93.89 ± 0.91
							Integrated age = 92.4 ± 0.4 Ma
CA99-7 biotite single grain							
1	44.30	4.44	667.0 ± 18.1	5.53 ± 0.01	0.0032 ± 0.0002	3.066 ± 0.071	95.28 ± 2.17
2	15.47	13.21	1909.1 ± 71.1	3.66 ± 0.01	0.0038 ± 0.0001	3.079 ± 0.023	95.68 ± 0.72
3	4.34	16.92	6788.8 ± 707.6	3.27 ± 0.01	0.0042 ± 0.0001	3.109 ± 0.016	96.59 ± 0.51
4	6.88	9.52	4286.7 ± 472.2	3.30 ± 0.01	0.0063 ± 0.0001	3.060 ± 0.026	95.10 ± 0.81
5	5.81	9.37	5071.5 ± 609.1	3.33 ± 0.01	0.0054 ± 0.0001	3.122 ± 0.025	96.97 ± 0.76
6	6.40	14.13	4594.2 ± 345.5	3.29 ± 0.01	0.0110 ± 0.0001	3.069 ± 0.018	95.37 ± 0.55
7	7.53	3.67	3915.7 ± 895.1	3.37 ± 0.01	0.0067 ± 0.0003	3.098 ± 0.060	96.25 ± 1.81
8	3.58	6.84	8215.7 ± 2923.8	3.26 ± 0.01	0.0094 ± 0.0002	3.131 ± 0.043	97.24 ± 1.32
9	0.97	4.88	29793.6 ± 4297.8	3.21 ± 0.01	0.0102 ± 0.0003	3.168 ± 0.049	98.39 ± 1.49
10	6.09	2.03	4828.1 ± 3148.2	3.20 ± 0.01	0.0120 ± 0.0006	2.994 ± 0.130	93.09 ± 3.96
11	3.04	3.34	9647.5 ± 8942.1	3.20 ± 0.01	0.0086 ± 0.0004	3.084 ± 0.093	95.80 ± 2.82
Fuse	2.60	11.65	11335.6 ± 2974.4	3.17 ± 0.01	0.0042 ± 0.0001	3.069 ± 0.023	95.39 ± 0.70
							Integrated age = 96.0 ± 0.3 Ma
CA99-7 biotite single grain							
1	92.77	1.12	318.9 ± 4.2	38.65 ± 0.16	0	2.875 ± 0.552	89.49 ± 16.79
2	83.61	2.13	353.6 ± 3.6	20.00 ± 0.07	0	3.303 ± 0.218	102.44 ± 6.57
3	68.93	6.65	429.0 ± 2.7	10.13 ± 0.01	0	3.164 ± 0.072	98.23 ± 2.20
4	28.26	9.04	1045.5 ± 26.6	4.26 ± 0.01	0	3.063 ± 0.035	95.18 ± 1.08
5	15.27	9.52	1928.3 ± 127.2	3.67 ± 0.01	0.0247 ± 0.0002	3.111 ± 0.040	96.62 ± 1.21
6	13.3	8.16	2217.5 ± 219.3	3.60 ± 0.01	0.0109 ± 0.0002	3.125 ± 0.051	97.06 ± 1.55
7	20.27	7.19	1458.4 ± 59.7	3.90 ± 0.01	0	3.118 ± 0.036	96.84 ± 1.11
8	18.44	9.43	1601.8 ± 68.5	3.88 ± 0.01	0.0027 ± 0.0001	3.168 ± 0.033	98.36 ± 1.02
9	20.00	6.01	1475.8 ± 90.4	3.90 ± 0.01	0.0108 ± 0.0001	3.129 ± 0.051	97.19 ± 1.55
10	23.56	5.74	1253.6 ± 71.1	3.94 ± 0.01	0.0066 ± 0.0002	3.020 ± 0.056	93.90 ± 1.70
11	20.22	7.30	1470.7 ± 78.8	3.83 ± 0.01	0	3.069 ± 0.044	95.39 ± 1.36
12	20.52	9.65	1438.2 ± 52.6	3.80 ± 0.01	0.0104 ± 0.0001	3.027 ± 0.031	94.10 ± 0.96
13	15.10	12.74	1958.8 ± 88.9	3.65 ± 0.01	0	3.103 ± 0.029	96.40 ± 0.88
Fuse	19.91	5.31	1479.8 ± 120.3	3.73 ± 0.02	0.0271 ± 0.0003	2.998 ± 0.065	93.21 ± 1.98
							Integrated age = 96.2 ± 0.4 Ma
CA99-7 amphibole single grain							
1	82.73	0.49	346.4 ± 39.7	27.80 ± 0.65	8.715 ± 0.210	4.999 ± 2.837	152.84 ± 83.18
2	62.91	4.10	452.9 ± 25.2	8.98 ± 0.06	2.548 ± 0.160	3.360 ± 0.340	104.16 ± 10.26
3	71.88	2.66	396.7 ± 27.6	11.96 ± 0.06	3.795 ± 0.020	3.407 ± 0.647	105.55 ± 19.47
4	79.6	21.14	335.6 ± 2.6	13.97 ± 0.03	14.411 ± 0.047	3.200 ± 0.124	99.31 ± 3.75
5	23.25	23.73	542.7 ± 10.2	3.40 ± 0.10	12.96 ± 0.044	2.935 ± 0.049	91.30 ± 1.51
6	16.10	25.67	689.0 ± 23.1	3.23 ± 0.10	10.56 ± 0.032	3.016 ± 0.055	93.77 ± 1.69
7	13.28	10.25	817.0 ± 110.1	3.43 ± 0.10	9.591 ± 0.039	3.149 ± 0.176	97.78 ± 5.35
Fuse	15.79	11.98	779.2 ± 35.5	8.66 ± 0.30	23.604 ± 0.087	7.705 ± 0.170	230.50 ± 4.80
							Integrated age = 112.7 ± 1.5 Ma
CA99-3 biotite single grain							
1	81.50	0.21	359.4 ± 73.5	11.15 ± 0.30	0.9510 ± 0.0230	2.065 ± 1.932	64.66 ± 59.45
2	62.25	12.06	474.5 ± 11.9	8.74 ± 0.17	0.0153 ± 0.0003	3.294 ± 0.188	102.09 ± 5.69

(*continued overleaf*)

Table 3. (*continued*)

Step number or T (°C)	Atmospheric contamination (%)	^{39}Ar (%)	^{40}Ar/^{36}Ar	^{40}Ar/^{39}Ar	$^{37}Ar_{Ca}/^{39}Ar_K$	$^{40}Ar^*/^{39}Ar_K$	Age (Ma)
3	18.49	10.85	1594.8 ± 92.1	3.63 ± 0.09	0.0165 ± 0.0004	2.952 ± 0.092	91.74 ± 2.79
4	9.72	10.25	3040.4 ± 346.5	3.46 ± 0.07	0	3.123 ± 0.074	96.91 ± 2.25
5	15.76	9.51	1876.2 ± 170.6	3.87 ± 0.10	0	3.249 ± 0.108	100.72 ± 3.26
6	23.18	6.61	1274.0 ± 156.2	3.83 ± 0.11	0.0059 ± 0.0005	2.934 ± 0.150	91.20 ± 4.57
7	21.15	1.73	1395.4 ± 578.1	4.19 ± 0.03	0.0118 ± 0.0015	3.297 ± 0.378	102.18 ± 11.40
8	17.66	2.06	1669.1 ± 930.6	3.84 ± 0.01	0.0200 ± 0.0012	3.153 ± 0.389	97.83 ± 11.75
9	11.01	5.38	2680.8 ± 911.6	3.61 ± 0.01	0.0056 ± 0.0006	3.202 ± 0.139	99.31 ± 4.21
10	21.36	6.41	1381.5 ± 143.7	3.72 ± 0.01	0.0126 ± 0.0005	2.915 ± 0.085	90.63 ± 2.60
11	19.01	6.77	1554.2 ± 181.5	3.66 ± 0.01	0.0001 ± 0.0005	2.956 ± 0.084	91.88 ± 2.55
12	27.25	3.93	1082.5 ± 140.1	3.81 ± 0.01	0.0220 ± 0.0010	2.765 ± 0.138	86.07 ± 4.22
13	18.90	5.71	1565.1 ± 243.0	3.82 ± 0.01	0	3.090 ± 0.115	95.93 ± 3.49
Fuse	18.72	18.54	1578.5 ± 74.7	3.80 ± 0.01	0.0019 ± 0.0002	3.079 ± 0.036	95.60 ± 1.10
							Integrated age = 95.7 ± 0.4 Ma
CA99-3 amphibole single grain							
1	97.86	3.16	301.5 ± 1.5	173.3 ± 1.22	2.970 ± 0.024	3.913 ± 1.437	120.63 ± 42.88
2	91.58	12.97	317.6 ± 2.7	35.82 ± 0.08	6.418 ± 0.026	3.118 ± 0.363	96.76 ± 10.99
3	68.07	26.2	369.7 ± 4.0	9.26 ± 0.01	13.429 ± 0.049	3.147 ± 0.101	97.64 ± 3.06
4	23.32	27.65	585.4 ± 21.9	3.68 ± 0.01	12.191 ± 0.045	3.008 ± 0.078	93.43 ± 2.39
5	37.23	4.46	497.1 ± 63.8	3.98 ± 0.01	10.777 ± 0.048	2.647 ± 0.315	82.47 ± 9.60
6	39.13	3.45	473.0 ± 80.2	3.92 ± 0.02	11.183 ± 0.075	2.547 ± 0.431	79.44 ± 13.16
7	68.76	1.21	323.2 ± 94.1	4.43 ± 0.03	12.271 ± 0.068	1.528 ± 1.221	48.06 ± 37.93
8	86.62	1.14	297.2 ± 42.4	9.27 ± 0.06	14.520 ± 0.110	1.393 ± 1.365	43.87 ± 42.49
9	56.61	1.46	368.3 ± 125.4	5.93 ± 0.05	17.191 ± 0.150	2.767 ± 1.686	86.13 ± 51.26
10	43.29	1.15	426.1 ± 161.0	4.98 ± 0.04	15.908 ± 0.120	3.027 ± 1.356	94.00 ± 41.04
Fuse	46.24	17.14	434.0 ± 10.8	5.01 ± 0.02	13.359 ± 0.064	2.889 ± 0.097	89.85 ± 2.94
							Integrated age = 93.1 ± 2.6 Ma
CA99-3 amphibole single grain							
1	96.45	0.85	306.1 ± 2.5	384.1 ± 5.99	3.688 ± 0.060	14.84 ± 3.73	420.06 ± 94.10
2	96.22	1.31	305.2 ± 11.4	37.71 ± 0.32	2.774 ± 0.024	1.618 ± 1.429	50.85 ± 44.31
3	67.57	1.53	424.0 ± 88.5	6.75 ± 0.07	1.743 ± 0.018	2.258 ± 1.021	70.56 ± 31.32
4	92.25	3.09	317.3 ± 5.6	56.31 ± 0.30	5.955 ± 0.035	4.559 ± 1.011	139.74 ± 29.82
5	90.56	15.43	308.7 ± 2.7	27.45 ± 0.06	17.294 ± 0.058	3.177 ± 0.277	98.52 ± 8.38
6	43.31	16.21	422.5 ± 13.8	4.69 ± 0.02	15.276 ± 0.069	3.159 ± 0.120	97.98 ± 3.62
7	27.00	16	518.3 ± 26.8	3.69 ± 0.01	13.536 ± 0.051	3.165 ± 0.119	98.15 ± 3.61
8	28.30	13.21	513.0 ± 31.5	3.50 ± 0.01	12.518 ± 0.062	2.964 ± 0.134	92.08 ± 4.07
9	39.10	10.35	435.5 ± 26.4	4.25 ± 0.02	14.958 ± 0.062	3.056 ± 0.188	94.85 ± 5.70
Fuse	40.49	22.02	407.6 ± 9.8	4.17 ± 0.01	16.348 ± 0.065	3.030 ± 0.088	94.08 ± 2.66
							Integrated age = 99.4 ± 2.4 Ma
CA99-6 amphibole single grain							
1	94.51	0.89	311.9 ± 5.2	39.73 ± 0.39	1.058 ± 0.011	2.388 ± 0.676	74.64 ± 20.71
2	49.67	2.70	570.6 ± 17.1	5.45 ± 0.02	1.396 ± 0.006	2.732 ± 0.091	85.15 ± 2.77
3	46.66	2.84	622.5 ± 38.8	5.33 ± 0.03	0.521 ± 0.003	2.824 ± 0.166	87.94 ± 5.07
4	47.23	3.80	601.0 ± 15.2	6.12 ± 0.01	1.439 ± 0.005	3.238 ± 0.082	100.47 ± 2.48
5	67.32	3.84	410.6 ± 7.96	9.17 ± 0.02	5.184 ± 0.017	3.116 ± 0.138	96.78 ± 4.20
6	35.28	18.4	549.2 ± 6.85	4.31 ± 0.01	9.728 ± 0.026	3.086 ± 0.040	95.88 ± 1.22
7	13.34	28.66	818.6 ± 14.4	3.14 ± 0.01	8.704 ± 0.025	3.022 ± 0.030	93.93 ± 0.93
8	5.09	5.65	2003.3 ± 324.1	3.15 ± 0.01	3.689 ± 0.013	3.070 ± 0.079	95.40 ± 2.40
9	9.89	7.14	1398.1 ± 113.5	3.24 ± 0.01	4.427 ± 0.013	3.006 ± 0.059	93.46 ± 1.80
10	9.49	6.86	1336.0 ± 99.4	3.23 ± 0.01	4.964 ± 0.022	3.041 ± 0.058	94.51 ± 1.76
Fuse	8.58	19.21	1609.0 ± 55.2	3.11 ± 0.01	3.697 ± 0.011	2.924 ± 0.023	90.97 ± 0.71
							Integrated age = 93.6 ± 0.5 Ma
CA99-4 cluster of amphibole (4 grains)							
1	86.39	0.14	338.9 ± 28.7	18.46 ± 0.50	1.754 ± 0.018	2.669 ± 1.421	85.14 ± 44.29
2	96.84	0.10	301.6 ± 63.0	9.09 ± 0.20	1.214 ± 0.012	0.308 ± 1.932	10.02 ± 62.78
3	42.83	0.14	659.4 ± 413.1	6.73 ± 0.11	1.702 ± 0.017	4.063 ± 2.062	128.05 ± 62.76
4	27.25	0.84	799.0 ± 169.4	3.87 ± 0.02	4.571 ± 0.046	2.916 ± 0.316	92.82 ± 9.82
5	24.00	1.25	826.1 ± 125.6	3.75 ± 0.01	5.366 ± 0.055	2.967 ± 0.213	94.41 ± 6.61
6	12.60	3.68	1024.7 ± 52.5	3.19 ± 0.01	6.298 ± 0.064	2.903 ± 0.052	92.41 ± 1.62
7	17.54	6.93	895.3 ± 20.7	3.41 ± 0.01	6.434 ± 0.065	2.939 ± 0.032	93.55 ± 1.01
8	13.22	4.69	1084.4 ± 46.0	3.20 ± 0.01	5.459 ± 0.055	2.895 ± 0.041	92.18 ± 1.30
9	12.36	12.91	1136.2 ± 25.7	3.20 ± 0.01	5.319 ± 0.054	2.918 ± 0.024	92.89 ± 0.77
10	10.24	15.55	1218.9 ± 26.0	3.16 ± 0.01	5.389 ± 0.055	2.950 ± 0.022	93.88 ± 0.71
11	9.64	20.62	1234.8 ± 17.4	3.15 ± 0.01	5.469 ± 0.056	2.951 ± 0.018	93.90 ± 0.59
12	24.66	2.46	817.6 ± 58.0	3.77 ± 0.02	5.257 ± 0.053	2.942 ± 0.102	93.62 ± 3.19
13	9.22	8.70	1327.2 ± 44.0	3.13 ± 0.01	4.974 ± 0.051	2.947 ± 0.027	93.77 ± 0.87
Fuse	8.87	21.97	1358.9 ± 23.5	3.13 ± 0.01	4.906 ± 0.050	2.963 ± 0.018	94.28 ± 0.57
							Integrated age = 93.6 ± 0.3 Ma

(*continued*)

Table 3. (*continued*)

Step number or T (°C)	Atmospheric contamination (%)	^{39}Ar (%)	^{40}Ar/^{36}Ar	^{40}Ar/^{39}Ar	$^{37}Ar_{Ca}/^{39}Ar_K$	$^{40}Ar^*/^{39}Ar_K$	Age (Ma)
CA99-3 plagioclase bulk sample							
550	98.76	0.09	299.1 ± 1.3	299.7 ± 1.60	0.590 ± 0.004	4.569 ± 1.991	140.23 ± 58.80
650	94.5	0.64	312.4 ± 1.2	62.60 ± 0.12	0.529 ± 0.002	4.189 ± 0.385	128.95 ± 11.45
700	73.85	1.68	398.7 ± 2.1	12.38 ± 0.02	0.387 ± 0.001	3.383 ± 0.071	104.84 ± 2.14
750	48.89	2.47	593.8 ± 8.3	5.99 ± 0.01	0.634 ± 0.002	3.038 ± 0.046	94.42 ± 1.42
800	32.00	5.06	896.9 ± 6.5	4.40 ± 0.01	0.503 ± 0.001	2.964 ± 0.016	92.17 ± 0.49
850	19.33	5.92	1435.4 ± 19.6	3.69 ± 0.01	0.560 ± 0.001	2.945 ± 0.013	91.61 ± 0.40
900	14.00	13.39	1971.0 ± 14.3	3.57 ± 0.01	0.428 ± 0.001	3.034 ± 0.008	94.32 ± 0.26
950	9.46	8.41	2932.0 ± 48.9	3.36 ± 0.01	0.254 ± 0.001	3.02 ± 0.008	93.88 ± 0.27
1000	48.37	10.2	607.4 ± 1.9	5.95 ± 0.01	0.206 ± 0.001	3.044 ± 0.022	94.61 ± 0.68
1050	24.35	11.52	1189.9 ± 8.2	4.05 ± 0.01	0.239 ± 0.001	3.037 ± 0.012	94.38 ± 0.38
1100	29.01	8.65	999.3 ± 7.3	4.27 ± 0.01	0.291 ± 0.001	3.009 ± 0.014	93.55 ± 0.44
1150	21.41	20.54	1351.6 ± 8.0	3.86 ± 0.01	0.213 ± 0.001	3.009 ± 0.010	93.53 ± 0.31
1200	25.86	7.46	1105.8 ± 13.0	4.13 ± 0.01	0.434 ± 0.001	3.037 ± 0.016	94.40 ± 0.51
1250	55.89	1.71	507.1 ± 4.2	6.94 ± 0.01	1.991 ± 0.006	3.125 ± 0.042	97.05 ± 1.28
1200	71.97	0.64	398.5 ± 5.0	10.61 ± 0.01	2.809 ± 0.008	3.222 ± 0.109	99.99 ± 3.31
1400	88.81	1.03	330.1 ± 1.7	24.83 ± 0.05	2.162 ± 0.007	3.915 ± 0.165	120.80 ± 4.94
Fuse	93.46	0.61	315.4 ± 1.7	41.56 ± 0.08	1.232 ± 0.004	4.371 ± 0.296	134.35 ± 8.78
							Integrated age = 94.9 ± 0.2 Ma

^{40}Ar* is radiogenic ^{40}Ar; subscripts Ca and K indicate produced by Ca and K neutron interference, respectively. All ratios are corrected for mass discrimination. Correction factors for interfering isotopes are $(^{39}Ar/^{37}Ar)_{Ca} = 7.06 \times 10^{-4}$, $(^{36}Ar/^{37}Ar)_{Ca} = 2.79 \times 10^{-4}$, and $(^{40}Ar/^{39}Ar)_K = 2.97 \times 10^{-2}$. Uncertainties are given at the 1σ level.

Table 4. *Summary of the apatite fission-track count data*

Sample	Zone	Grains	ρ(s)	N(s)	ρ(i)	N(i)	χ^2	ρ(d)	N(d)	Age ± error (Ma, 2σ)
970118-3	GDZ	27	16.6	2482	32.9	4903	0.2701	1043	8000	92.7 ± 6.2
CA99-1	GDZ	20	1138	2300	2458	4965	100	145	6820	93.1 ± 2.6
970121-4	TZ	20	12.7	1165	25.7	2360	0.5652	1043	8000	90.4 ± 7.6
970524-3	TZ	26	16.2	2723	31	5206	0.4339	1043	8000	95.7 ± 6.2
CA99-7	TZ	7	2022	497	4211	1035	65	1145	6820	96.5 ± 5.4
CA99-4	GZ	17	0.96	4.88	2099	1067	22	1145	6820	91.9 ± 5.1
970616-1	GZ	28	10.5	2275	23.5	5082	0.9811	1043	8000	82.0 ± 5.6

All samples pass the χ^2 test at the 95% confidence level (i.e. are composed of one age population). Sample ages are calculated using pooled statistics. N(s), N(i) and N(d) are the numbers of spontaneous, induced and flux dosimeter (CN-5) tracks, respectively. ρ(s), ρ(i) and ρ(d) are the density of spontaneous, induced and dosimeter tracks, respectively. A value of 353.5 ± 7.1 (CN-5) was used for zeta factor. Age error estimates are at the 95% (2σ) confidence level. Analyses by A. M. Grist (Dalhousie University).

length data represent a single modelable history. Figure 7 shows the preferred calculated thermal history (cooling-only model) for the three samples since 100 Ma. The results indicate that the samples appear to have cooled at *c*. 90 Ma from temperatures high enough to cause substantial apatite fission-track annealing, and have not subsequently experienced any significantly elevated temperatures. A cooling rate of 5 °C Ma^{-1} is obtained from Figure 6 for the 100–80 Ma interval. No significant variation in the very slow cooling rate is apparent after 80 Ma, as shown in Figure 7.

In conclusion, if the fission-track model is correct, it suggests exhumation of the pluton and host rocks between about 94 and 90 Ma. Nevertheless, our data do not allow us to determine whether the exhumation of the pluton occurred continuously along cooling path A (Fig. 6), as it cooled from its level of emplacement, or episodically following cooling path B as a result of intermediate temperature stabilization with a significant break in the cooling curve. The coincidence in time between the exhumation of the pluton and the deposition of the thick strata of conglomerates and breccias (molasse-type deposits) of the upper section of the Las Chilcas Formation (Fig. 2) suggests a cause-and-effect relationship.

Discussion: plutonism during a shift from an extensional to a compressional regime

Extension during Caleu magma generation

An extensional tectonic regime and associated crustal attenuation during the Early Cretaceous has been documented along the Pacific margin of South America (e.g. Dalziel 1981; Atherton *et al*. 1983), probably related to an episode of slow sea-floor spreading (Larson & Pitman 1972), which, in turn, conditioned a Mariana-type subduction (e.g. Pankhurst *et al*. 1988) associated with a trench retreat (roll-back effect). Along the central Chilean margin, the crustal attenuation developed progressively since the early Mesozoic (Vergara *et al*. 1995; Parada *et al*. 1999) and culminated with an aborted marginal basin where the thickest volcanic and sedimentary sucessions were deposited during the Early Cretaceous (Åberg *et al*. 1984). The progressive extension in the segment studied would be reflected in magmas exhibiting isotopic (Sr–Nd) secular variations from an enriched lithospheric-dominated mantle source of the late Palaeozoic plutonism (Parada *et al*. 1999), to a depleted asthenospheric-dominated source of the mid-Cretaceous Caleu-type magmatism (Fig. 8). The increasing isotopic depletion of the Mesozoic magmatism

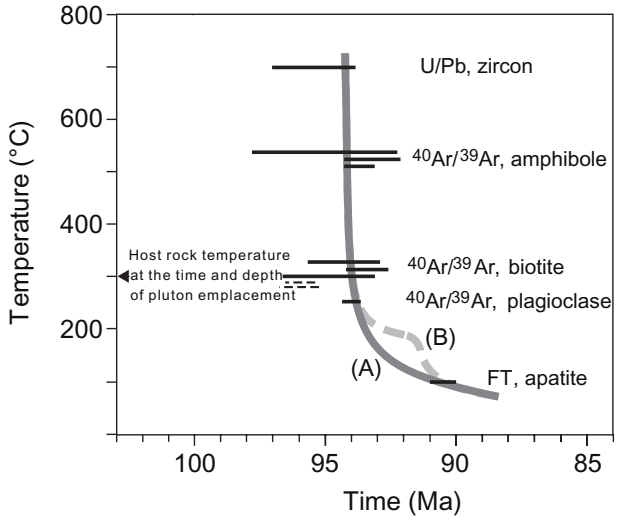

Fig. 6. Cooling history of the Caleu pluton, as deduced from geochronological data. The U–Pb age range is based on the spread of data along the concordia curve. Error bars on $^{40}Ar/^{39}Ar$ plateau ages are given at the 2σ confidence level. For biotite, dashed lines represent older ages obtained on a sample (CA99-7) from the margin of the pluton (see text). The restricted indicated age range for the fission tracks is deduced from a thermal model (see text). The indicated closure temperature for each mineral (taken from Berger & York 1981; McDougall & Harrison 1999) and chronometer is approximate, and no error bar is given. The fast cooling of the pluton started coevally with its emplacement and ended when pluton and host rocks cooled together to *c*. 250° C as a result of exhumation. The slower cooling to *c*. 100° C could be continuous (curve A) or episodic (curve B) according to the rate of the concomitant exhumation.

with decreasing age can be explained by a progressive removal of the mantle lithosphere as a result of a continuous asthenospheric upwelling that accompanied extension. Thus, the Caleu magma, the most depleted of all, would have been formed when extension reached its maximum.

Exhumation during compressional deformation

The exhumation of the Caleu pluton is part of a more regional-scale mid-Cretaceous exhumation in the Coastal Batholith of central Chile (32°30′S–33°30′S). In fact, an exhumation event of the late Palaeozoic, Mid-Jurassic and Early Cretaceous granitoids of this batholith during the interval 106–90 Ma (Gana & Zentilli 2000; this study) has also been identified by means of fission-track dating. The magnitude of this exhumation was stronger along the present-day coastline where the deep-seated (*c*. 3.0–5.5 kbar or *c*. 12–20 km depth based on Al-in-hornblende geobarometry; Gana & Tosdal 1996; Sial *et al*. 1999) late Palaeozoic to Mid-Jurassic plutono-metamorphic belt is now exposed.

It is well known that deep-seated orogenic terranes can be exhumed during extension associated with collapse of a thickened crust (see Dewey 1988; Liu & Shen 1998), or during convergent deformation and erosion (see Stüwe & Barr 1998). In the studied case, the crustal thickness prior to the Early Cretaceous would have been <40 km as suggested by the low La/Yb ratios, typical of a garnet-free source (equilibrated at <10 kbar; Rutter & Wyllie 1988; Rapp & Watson 1995), observed in late Palaeozoic and Jurassic I-type granitoids (López-Escobar *et al*. 1979; Parada *et al*. 1991, 1999). This crustal thickness estimate is below the >50 km needed to produce dynamic instability capable of driving collapse of the crust (see Liu & Shen 1998). It is then possible to infer that the cause of the exhumation of the studied coastal segment can be attributed to a change in the tectonic regime identified at these latitudes in the Coastal Range and along the Chile–Argentina Andes, during the mid-Cretaceous. At this time, extensional tectonics ended and a high-stress compressional regime started, giving rise to: (1) the roughly north–south Silla del Gobernador contractional shear zone (Arancibia 2002), recently dated at 97.8 ± 1.5 Ma (Arancibia, pers. commun.), in the western boundary of the Coastal Range, *c*. 150 km north of the Caleu pluton; (2) the shortening that generated the mid- to Late Cretaceous Agrio and Aconcagua fold–thrust belts located in the central High Andes of Argentina and Chile (Mpodozis & Ramos 1989; Ramos & Aleman 2000). Mid-Cretaceous basin inversion and folding (Mochica event) have also been recognized in western Peru (Atherton 1990).

An abrupt upward shift of the sedimentary facies in the Las Chilcas Formation exists, from limestones and sandstones, in the lower section, to a coarsening upward clastic succession in the upper section culminating with thick (30–50 m) strata of very coarse (up to 50 cm long clasts) sedimentary breccias and conglomerates (deposited coevally with the Caleu pluton emplacement). This feature is indicative of an abrupt change in the sedimentary regime with time. In fact, limestones of the lower section are marine and correspond to a transgressive open carbonate shelf (Martínez-Pardo *et al*. 1994), whereas the clastic rocks of the upper section could represent a syntectonic molasse deposit that accompanied tectonic basin inversion.

Final considerations

It is worth noting the similarities and differences between the Early Cretaceous rifted continental margin evolution of the West Peruvian Trough (Atherton 1990; Petford & Atherton 1995) and the contemporaneous evolution of this Chilean Coastal Range segment. In both cases, the sequence of events started with extensional basin magmatism and culminated in emplacement of plutons, passing through basin subsidence. However, the Coastal Batholith of Peru is considered to have been derived from partial melting of a 'new crust' (Atherton 1990). In contrast, the Caleu-type plutonism cannot be considered as a product of recycling of young lower mafic crust, whose upper-crustal equivalents would be the Veta Negra basaltic rocks. In fact, this assumption is not tenable as the Caleu pluton is isotopically more depleted than the Veta Negra volcanic rocks (Fig. 8).

Finally, it is conceivable that the Caleu plutonism is the turning point between an extensional and a compressional regime. This switch in geodynamic setting would have occurred during the time elapsed between the generation and emplacement of the Caleu magma, as suggested by: (1) the coincidence in the ages of the Caleu pluton emplacement and the climax of the non-deformational very low-grade burial metamorphism, which marks the end of subsidence; (2) the unroofing of the pluton since it was emplaced; (3) the contemporaneity between pluton emplacement and the sedimentary response to the basin inversion, represented by the syntectonic breccias and conglomerates (upper section of the Las Chilcas Formation), containing abundant metavolcanic clasts with very low-grade mineral assemblages. In summary, the Caleu magma would have been

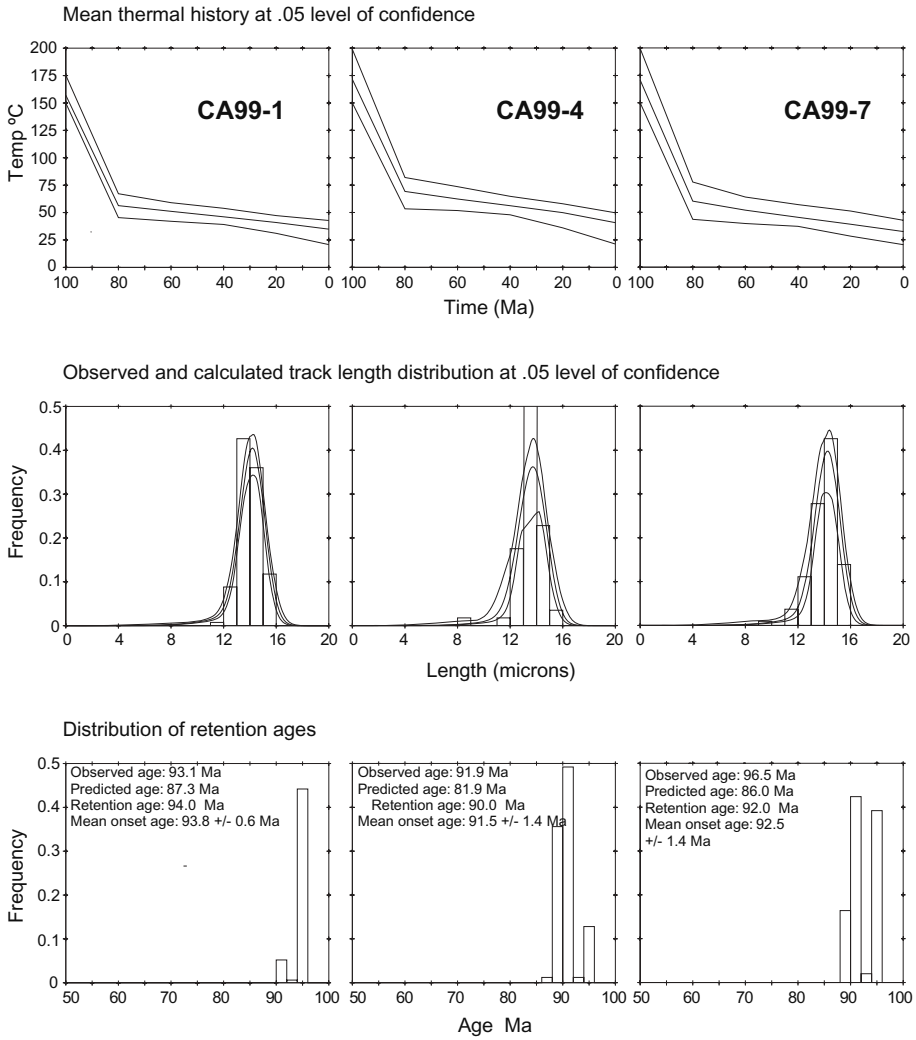

Fig. 7. Modelled thermal history of samples from the Caleu pluton based on apatite fission-track dataset (cooling-only model). The upper panel shows the calculated thermal history (middle curve) and the upper and lower bounding envelopes for 250 pre-determined solutions. The middle panel shows histograms of the measured distribution of confined fission track lengths. Overlying the histograms are curves for the calculated length distribution (middle curves). Also shown are the upper and lower bounding envelopes for all solutions. The lower panel shows histograms of the distribution of the times of initial onset of track retention (retention ages) for all solutions.

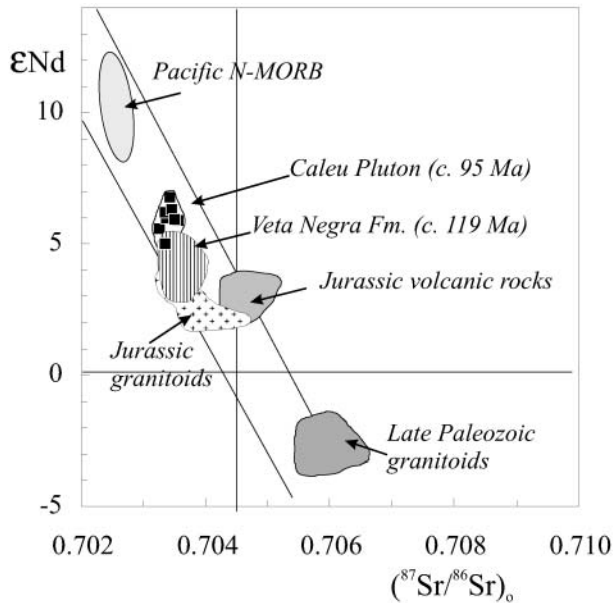

Fig. 8. ϵ_{Nd} v. initial $^{87}Sr/^{86}Sr$ ratios for mantle-derived granitoids and volcanic rocks of the studied Coastal Range segment. Pacific N-MORB (normal mid-ocean ridge basalt) field after Peate *et al*. (1997). Fields of Late Palaeozoic and Jurassic granitoids are from Parada *et al*. (1999). Fields of Veta Negra Formation and Jurassic volcanic rocks are from Morata *et al*. (2001). Data for the Caleu pluton after Parada *et al*. (2002).

generated during the climax of the Early Cretaceous extension and emplaced during the beginning of basin inversion.

This study was mainly financed by FONDECYT grant 1990980. Additional funds were provided by two CNRS–CONICYT grants (1999 and 2000), FONDEF grant 1033 and FONDECYT grant 1031000. We thank J. Richards, R. Tosdal and M. Villeneuve for constructive reviews of the original manuscript. This paper is Contribution Geosciences Azur number 658.

References

Åberg, G., Aguirre, L., Levi, B. & Nyström, J.O. 1984. Spreading–subsidence and generation of ensialic marginal basins: an example from the Early Cretaceous of central Chile. *In:* Kokelaar, B.P. & Howells, M.F. (eds) *Volcanic and Associated Sedimentary and Tectonic Processes in Modern and Ancient Marginal Basins*. Geological Society, London, Special Publications, **16**, 185–193.

Aguirre, L., Levi, B. & Nyström, J.O. 1989. The link between metamorphism, volcanism and geotectonic setting during the evolution of the Andes. *In:* Daly, J.S., Cliff, R.A. & Yardley, B.W.D. (eds) *Evolution of Metamorphic Belts*. Geological Society, London, Special Publications, **43**, 223–232.

Aguirre, L., Feraud, G., Morata, D., Vergara, M. & Robinson, D. 1999. Time interval between volcanism and burial metamorphism and rate of basin subsidence in a Cretaceous Andean extensional basin. *Tectonophysics*, **313**, 433–447.

Arancibia, G. 2002. Mid-Cretaceous crustal shortening, uplift and exhumation: evidence from a regional-scale ductile shear zone in the Coastal Range of central Chile (32°S). *In: 5th International Symposium on Andean Geodynamics, Toulouse, France, Extended Abstract Volume*. 33–36.

Atherton, M.P. 1990. The Coastal Batholith of Peru: the product of rapid recycling of 'new' crust formed within rifted continental margin. *Geological Journal*, **25**, 337–349.

Atherton, M.P., Pitcher, W.S. & Warden, V. 1983. The Mesozoic marginal basin of Central Peru. *Nature*, **305**, 303–306.

Atherton, M.P., Warden, V. & Sanderson, L.M. 1985. The Mesozoic marginal basin of Central Peru: a geochemical study of within plate edge volcanism. *In:* Pitcher, W.S., Atherton, M.P., Cobbing, E.J. & Beckinsale, R.D. (eds) *Magmatism at a Plate Edge: the Peruvian Andes*. Blackie Halsted, Glasgow, 47–58.

Barton, M.D. & Hanson, R.B. 1989. Magmatism and the development of low-pressure metamorphic belts: implications from the western United States and thermal modeling. *Geological Society of America Bulletin*, **101**, 1051–1065.

Berger, G.W. & York, D. 1981. Geothermometry from $^{40}Ar/^{39}Ar$ dating experiments. *Geochimica et Cosmochimica Acta*, **45**, 795–811.

Dalziel, I.W.D. 1981. Back-arc extension in the southern Andes: a review and critical reappraisal. *Philosophical Transactions of the Royal Society of London, Series A*, **300**, 319–335.

Dewey, J.F. 1988. Extensional collapse of orogens. *Tectonics*, **7**, 1123–1139.

England, P.C. & Molnar, P. 1990. Surface uplift, uplift of rocks and exhumation of rocks. *Geology*, **18**, 1173–1177.

Fleisher, R.L., Price, P.B. & Walker, R.M. 1975. *Nuclear Tracks in Solids: Principles and Applications*. University of California Press, Berkeley, CA, 605.

Fuentes, F., Féraud, G., Aguirre, L. & Morata, D. 2001. Convergent strategy to date metamorphic minerals in subgreenschist facies metabasites by the $^{40}Ar/^{39}Ar$ method. *In: 3th South American Symposium on Isotope Geology, Pucón. Extended. Abstract Volume (CD)* 34–36.

Gana, P. & Tosdal, R.M. 1996. Geocronología U–Pb y K–Ar en intrusivos del Paleozoico y Mesozoico de la Cordillera de la Costa, región de Valparaíso, Chile. *Revista Geológica de Chile*, **23**, 151–164.

Gana, P. & Zentilli, M. 2000. Historia termal y exhumación de intrusivos de la Cordillera de la Costa de Chile central. *In: IX Congreso Geológico Chileno, Puerto Varas. Symposio Internacional sobre Magmatismo Andino, Actas*, **2**, 664–668.

Gana, P., Wall, R. & Gutierrez, A. 1996. *Mapa geológico del área de Valparaíso–Curacaví*. Escala 1:100 000. Servicio Nacional de Geología y Minería, Chile.

Hurford, A.J. & Green, P.F. 1982. A users guide to fission track dating calibration. *Earth and Planetary Science Letters*, **59**, 343–354.

Issler, D.I. 1996. *An inverse model for extracting thermal histories from apatite fission track data: instructions and software for the Window 95 environment*. Geological Survey of Canada, Open File Report, **2325**.

Larson, R.L. & Pitman, W.C. 1972. World-wide correlation of Mesozoic magnetic anomalies, and its implications. *Geological Society of America Bulletin*, **83**, 3645–3662.

Levi, B. 1969. Burial metamorphism of a Cretaceous volcanic sequence west from Santiago, Chille. *Contributions to Mineralogy and Petrology*, **24**, 30–49.

Levi, B. & Aguirre, L. 1981. Ensialic spreading–subsidence in the Mesozoic and Paleogene Andes of central Chile. *Journal of the Geological Society, London*, **138**, 75–81.

Levi, B., Aguirre, L. & Nystrom, J.O. 1982. Metamorphic gradients in burial metamorphosed vesicular lavas: comparison of basalt and spilite in Cretaceous basic flows from central Chile. *Contributions to Mineralogy and Petrology*, **80**, 49–58.

Levi, B., Nyström, J.O., Thiele, R. & Åberg, G. 1988. Facies de alteración regional en las secuencias volcánicas mesozoicas y cenozoicas de Chile central. *Revista Geológica de Chile*, **15**, 83–88.

Levi, B., Aguirre, L., Nyström, J.O., Padilla, H. & Vergara, M. 1989. Low-grade regional metamorphism in the Mesozoic–Cenozoic volcanic sequences of the Central Andes. *Journal of Metamorphic Geology*, **7**, 487–495.

Liu, M. & Shen, Y. 1998. Crustal collapse, mantle upwelling, and Cenozoic extension in the North American Cordillera. *Tectonics*, **17**, 311–321.

López-Escobar, L., Frey, F.A. & Oyarzún, J. 1979. Geochemical characteristics of Central Chile (33°–34°S) granitoids. *Contributions to Mineralogy and Petrology*, **70**, 439–450.

Lux, D.R., DeYoreo, J.J., Guidotti, C.V. & Decker, E.R. 1986. Role of plutonism in low-pressure metamorphic belt formation. *Nature*, **323**, 794–797.

Martínez-Pardo, R., Gallego, A. & Martinez-Guzman, R. 1994. Middle Albian marine planktonic microfossils from the Santiago basin, central Chile: their depositional and paleogeographic meaning. *Revista Geológica de Chile*, **21**, 173–187.

McDougall, I. & Harrison, T.M. 1999. *Geochronology and Thermochronology by the $^{40}Ar/^{39}Ar$ Method*. Oxford University Press, New York.

Morata, D., Aguirre, L., Féraud, G., Fuentes, F., Parada, M.A. & Vergara, M. 2001. The Lower Cretaceous volcanism in the Coastal Range of central Chile: geochronology and isotopic geochemistry. *In: 3rd South American Symposium on Isotope Geology, Pucón, Extended Abstract Volume (CD)* 321–324.

Mpodozis, C. & Ramos, V. 1989. The Andes of Chile and Argentina. *In:* Ericksen, G.E., Cañas Pinochet, M.T. & Reinemund, J.A. (eds) *Geology of the Andes and its Relation to Hydrocarbon and Mineral Resources*. Circum-Pacific Council for Energy and Mineral Resources, Earth Sciences Series, **11**, 59–90.

Pankhurst, R.J., Hole, M.J. & Brook, M. 1988. Isotope evidence for the origin of Andean granites. *Transactions of the Royal Society of Edinburgh: Earth Sciences*, **79**, 123–133.

Parada, M.A., Levi, B. & Nyström, J.O. 1991. Geochemistry of the Triassic to Jurassic plutonism of central Chile (30 to 33°S); petrogenetic implications and a tectonic discussion. *In:* Harmon, R.S. & Rapela, C.W. (eds) *Andean Magmatism and its Tectonic Setting*. Geological Society of America, Special Papers, **265**, 99–112.

Parada, M.A., Nyström, J.O. & Levi, B. 1999. Multiple sources for the Coastal Batholith of central Chile (31–34°S): geochemical and Sr–Nd isotopic evidence and tectonic implications. *Lithos*, **46**, 505–521.

Parada, M.A., Larrondo, P., Guiresse, C. & Roperch, P. 2002. Magmatic gradients in the Cretaceous Caleu pluton (central Chile): injections of pulses from a stratified magma reservoir. *Gondwana Research*, **5**, 307–324.

Peate, D.W., Pearce, J.A., Hawkesworth, C.J., Colley, H., Edwards, C.M.H. & Hirose, K. 1997. Geochemical variations in Vanuatu Arc lavas: the role of subducted material and a variable mantle wedge composition. *Journal of Petrology*, **38**, 1331–1358.

Petford, N. & Atherton, M. 1995. Crustal segmentation and the isotopic significance of the Abancay Deflection: Northern Central Andes (9–20°S). *Revista Geológica de Chile*, **22**, 235–243.

Pitcher, W.S. & Cobbing, E.J. 1985. Phanerozoic plutonism in the Peruvian Andes. *In:* Pitcher, W.W., Atherton, M.P., Cobbing, E.J. & Beckinsale, R.D. (eds) *Magmatism at a Plate Edge: the Peruvian Andes*. Blackie Halsted, Glasgow, 19–25.

Ramos, V. & Aleman, A. 2000. Tectonic evolution of the Andes. *In:* Cordani, U., Milani, E.J., Thomaz Filho, A. & Campos, D.A. (eds) *Tectonic Evolution of South America. 31st International Geological Congress, Rio de Janeiro*. Publisher, Town, 635–685.

Rapp, R.P. & Watson, E.B. 1995. Dehydration melting of metabasalt at 8–32 kbar: implications for continental growth and crust–mantle recycling. *Journal of Petrology*, **36**, 891–931.

Renne, P.R., Swisher, C.C., Deino, A.L., Karner, D.B., Owens, T. & DePaolo, D.J. 1998. Intercalibration of standards, absolute ages and uncertainties in $^{40}Ar/^{39}Ar$ dating. *Chemical Geology, Isotope Geoscience Section*, **145**, 117–152.

Ruffet, G., Féraud, G. & Amouric, M. 1991. Comparison of $^{40}Ar/^{39}Ar$ conventional and laser dating of biotites from the North Tregor Batholith. *Geochimica et Cosmochimica Acta*, **55**, 1675–1688.

Rutter, M.J. & Wyllie, P.J. 1988. Melting of vapor-absent tonalite at 10 kbar to simulate dehydration melting in the deep crust. *Nature*, **331**, 159–160.

Schmitz, M.D. & Bowring, S.A. 2001. U–Pb zircon and titanite systematics of the Fish Canyon Tuff: an assessment of high precision U–Pb geochronology and its application to young volcanic rocks. *Geochimica et Cosmochimica Acta*, **65**, 2571–2587.

Sial, A.N., Toselli, A.J., Saavedra, J., Parada, M.A. & Ferreira, V.P. 1999. Emplacement, petrological and magnetic susceptibility characteristics of diverse magmatic epidote-bearing granitoid rocks in Brazil, Argentina and Chile. *Lithos*, **46**, 367–392.

Stacey, J.S. & Kramers, J.D. 1975. Approximation of terrestial lead isotope evolution by a two-stage model. *Earth and Planetary Science Letters*, **26**, 207–221.

Stüwe, K. & Barr, T.D. 1998. On uplift and exhumation during convergence. *Tectonics*, **17**, 80–88.

Thomas, H. 1958. Geología de la Cordillera de la Costa entre el valle de La Ligua y la Cuesta de Barriga. *Instituto de Investigaciones Geológicas, Boletín*, **2**, 1–86.

Vergara, M., Levi, B., Nyström, J. & Cancino, A. 1995. Jurassic and Early Cretaceous island arc volcanism, extension, and subsidence in the Coast Range of central Chile. *Geological Society of America Bulletin*, **107**, 1427–1440.

Wall, R., Sellés, D. & Gana, P. 1999. *Area Tiltil–Santiago, región Metropolitana*. Escala 1:100 000. Servicio Nacional de Geología y Minería, Chile.

Willett, S.D. 1992. Modelling thermal annealing of fission tracks in apatite. *In:* Zentilli, M. & Reynolds, P.H. (eds) *Short Course Handbook on Low Temperature Thermochronology.* Mineralogy Association of Canada, Short Course Series, **20**, 43–72.

Willett, S.D. 1997. Inverse modelling of annealing fission tracks in apatite, I: A controlled random search method. *American Journal of Science*, **297**, 939–969.